Acta Mech
DOI 10.1007/s00707-016-1691-5

ORIGINAL PAPER

Giuseppe Failla · Francesco Paolo Pinnola · Gioacchino Alotta

Exact frequency response of bars with multiple dampers

Received: 17 March 2016 / Revised: 9 June 2016

Abstract The paper addresses the frequency analysis of bars with an arbitrary number of dampers, subjected to harmonically varying loads. Multiple external/internal dampers occurring at the same position along the bar, modelling external damping devices and internal damping due to damage or imperfect connections, are considered. In this context, the challenge is to handle simultaneous discontinuities of the response variables, i.e. axial force/displacement discontinuities at the location of external/internal dampers. Based on the theory of generalized functions, the paper will present exact closed-form expressions of the frequency response under point/polynomial loads, which hold regardless of the number of dampers. In addition, closed-form expressions will be derived for the exact dynamic stiffness matrix and load vector of the bar, to be used in a standard assemblage procedure for an exact frequency response analysis of 2D truss structures. Changes to consider a single damper at a given position are straightforward. Numerical applications show the advantages of the proposed method.

1 Introduction

The frequency response analysis of beam-like structures carrying viscoelastic dampers, and subjected to harmonically varying loads, has been the subject of several studies in the last decades [1–3]. While frequency response data play a crucial role for control design, finite element (FE) model updating, system, identification or damage detection [4–6], beams with viscoelastic dampers are of interest not only in vibration mitigation applications, but also to model dynamic interaction between beam and attached subsystems, and, in addition, flexibility and/or damping resulting from damage and imperfections [7–18]. In this context, there exist many applications where external and/or internal dampers act on axial vibrations of bars, as for instance to control vibrations of transmission elements in machineries [1] or pipe strings in deep sea mining systems [19], to counteract seismic-induced longitudinal vibrations of bridges [20], or to model damaged or imperfect joints between different parts [21–24]. In most applications, a classical Kelvin–Voigt viscoelastic model has been considered as constitutive law of dampers, consistently with FEMA code prescriptions.

The frequency analysis of axial vibrations under harmonic point or distributed loads has generally been pursued within a 1D formulation of the equation of motions. The frequency responses to arbitrarily placed unit point load and distributed load represent the so-called dynamic Green's function (DGF) and frequency

G. Failla
Dipartimento di Ingegneria Civile, dell'Ambiente, dell'Energia e dei Materiali (DICEAM), Università di Reggio Calabria, 89124 Reggio Calabria, Italy
E-mail: giuseppe.failla@unirc.it

F. P. Pinnola · G. Alotta (✉)
Dipartimento di Ingegneria Civile, Ambientale, Aerospaziale, dei Materiali (DICAM), Università di Palermo, Ed. 8, 90128 Palermo, Italy
E-mail: gioacchino.alotta@unipa.it

Published online: 29 July 2016

response function (FRF), respectively. Both can be computed by a classical exact approach, i.e. expressing the vibration response over every segment between consecutive positions of dampers/point load, as well as every segment under distributed load, in a trigonometric form involving two integration constants (and a particular integral for a segment under distributed load), totalling $2 \times k$ constants for k segments. The integration constants are computed by enforcing matching conditions between the responses over adjacent segments, along with the boundary conditions (B.C.). By this approach, however, the size of the coefficient matrix associated with the set of equations to be solved inevitably increases with the number of dampers. Also, it has to be re-inverted numerically for any forcing frequency of interest and updated whenever dampers or loads change positions. For these reasons, alternative exact or even approximate solutions have been sought. For the sake of generality, studies have generally attempted to derive analytical solutions, which may hold for any number of dampers.

The frequency analysis of bars with dampers has been addressed in some studies [25–32]. For a bar with an end viscous damper, Hull [25] built the exact DGFs in a closed form. Later, for bars with an arbitrary number of external grounded or attached mass dampers, and internal dampers, Failla [26] and Alati et al. [27] used generalized functions to build exact DGFs and FRFs under polynomial loads, by a direct integration method [26] or complex mode superposition [27]. Most studies on bars, however, focused on the free vibration response, proposing exact closed-form characteristic equations for some specific damping devices and configurations, such as a single in-span grounded damper in Ref. [28,29], a tip mass and a single in-span mass damper in Ref. [30], two in-span grounded dampers [31]. An approximate formulation of the eigenvalue problem has been pursued in Ref. [32] for a bar carrying a tip mass and several in-span mass dampers.

Since the combined use of several dampers is resorted to, for instance, vibration control under different excitation sources [9,10], and in recognition of the fact that dampers may model local damage or imperfect joints and connections [13,14,21–24], there exists an interest in frequency response solutions for bars where multiple dampers may occur simultaneously at the same location: an example could be an external damper applied at a bar section where an internal damper is also introduced to model flexibility/damping due to an imperfect connection or damage. On the other hand, it is noted that some studies have already investigated the bending response of beams with simultaneous occurrence of purely elastic external supports and internal joints [33,34]. For instance, using the theory of generalized functions Caddemi et al. [33] derived exact closed-form expressions for the static response of stepped Timoshenko beams carrying simultaneous external translational/rotational elastic supports and internal translational/rotational elastic joints, with feasible generalization to the axial problem. Likewise, the dynamic response under moving loads of multi-span stepped beams with simultaneous occurrence of external translational/rotational elastic supports and internal translational/rotational elastic joints has been studied by Xu and Li [34]. Further, the frequency response of Euler–Bernoulli beams with multiple external/internal translational and rotational dampers at the same position has recently been investigated by one of the authors [35]. Specifically, dampers with fractional-derivative constitutive law have been considered [35]. Exact closed-form FRFs have been derived under harmonically varying point/polynomial loads, for any number of dampers. In the same context, the exact dynamic stiffness matrix and load vector of the beam have been derived in a symbolic form, to be assembled for computing the frequency response of 2D frames with multiple dampers. For this purpose, the theory of generalized functions has been used [17,18,33,36–41]. Solutions in Ref. [35], however, have been obtained for beam bending vibrations only, and to the best of the authors' knowledge, no similar solutions are available for axial vibrations of bars.

Starting from Ref. [35], the purpose of this paper is to derive exact closed-form expressions for the frequency response of bars carrying an arbitrary number of multiple Kelvin–Voigt viscoelastic dampers at the same position, and subjected to harmonically varying point/polynomial loads. Based on this result, a new approach will be proposed to build the exact dynamic stiffness matrix and load vector of the bar with multiple dampers in analytical form, to be assembled for exact frequency response of 2D truss structures. It will be shown that the approach proposed in this paper and the previous one in Ref. [35] lead to the same exact dynamic stiffness matrix and load vector. However, once the nodal displacements are computed from the global dynamic stiffness matrix of the truss structure, the approach proposed in this paper proves computationally more efficient.

Upon describing the problem under study in Sect. 2, Sect. 3 will present the exact frequency response of the bar with multiple dampers under point/polynomial loads. Exact dynamic stiffness matrix and load vector will be presented in Sect. 4. A numerical application will be discussed in Sect. 5.

2 Bars under study

Consider the bar in Fig. 1. Let x be the longitudinal axis, L the total length, EA the axial rigidity, m_0 the mass per unit length. Symbol $u(x)$ denotes axial displacement of the cross section, and $n(x)$ is the axial force (Fig. 1

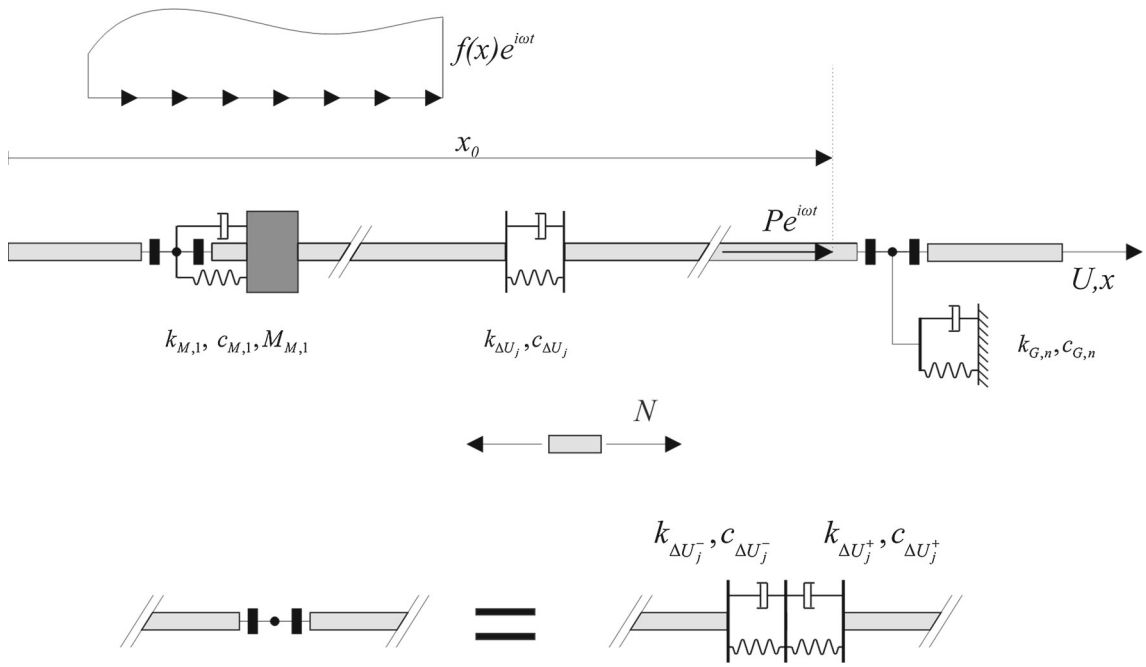

Fig. 1 *Bar* with multiple Kelvin–Voigt viscoelastic dampers at the same position

shows positive sign conventions). The bar carries an arbitrary number of external and internal dampers at n abscissas' x_j's along the axis, with Kelvin–Voigt viscoelastic law. For the jth damper, spring stiffness and dash-pot coefficients are indicated below.

- External dampers: $k_{G,j}, c_{G,j}$ for grounded dampers; $k_{M,j}, c_{M,j}$ for mass dampers, with M_j denoting the pertinent mass
- Internal dampers: $k_{\Delta U_j^{\pm}}, c_{\Delta U_j^{\pm}}$ for right and left dampers

Equations will be written for the most general case of external and internal dampers occurring simultaneously at the same location. Changes will be straightforward to consider a single damper at a given location, as shown later in the paper.

3 Axial frequency response

Assume that the bar is loaded by an axial harmonically varying distributed load $f(x)\,\mathrm{e}^{\mathrm{i}\omega t}$, over an interval (a, b) with $0 \leq a$ and $b \leq L$; ω is the frequency, and $\mathrm{i} = \sqrt{-1}$ is the imaginary unit. Representing the steady-state axial displacement and force as $u(x, \omega, t) = U(x, \omega)\,\mathrm{e}^{\mathrm{i}\omega t}$, $n(x, \omega, t) = N(x, \omega)\,\mathrm{e}^{\mathrm{i}\omega t}$, and using generalized functions to model discontinuous response variables, the following steady-state motion equation is derived [27,42]:

$$EA\frac{\bar{\mathrm{d}}^2 U(x)}{\mathrm{d}x^2} + R(x) + \Delta(x) + m_0\omega^2 U(x) + f(x) = 0, \tag{1}$$

where overbar means generalized derivative [36–38], while $R(x)$ and $\Delta(x)$ are generalized functions,

$$R(x) = \sum_{j=1}^{n} R_j \cdot \delta\left(x - x_j\right), \tag{2}$$

$$\Delta(x) = -\sum_{j=1}^{n} EA \cdot \Delta U_j \delta^{(1)}\left(x - x_j\right), \tag{3}$$

being $\delta\left(x - x_j\right)$ and $\delta^{(k)}\left(x - x_j\right)$ the Dirac's delta and its formal kth derivative at $x = x_j$, respectively [36–38]. Frequency dependence in Eqs. (1–3) is omitted for brevity.

In Eq. (2), R_j is the reaction of the jth external damper, for which the following relations hold:

$$R_j + N\left(x_j^+\right) = N\left(x_j^-\right), \tag{4}$$

$$R_j = -\left[\kappa_{G,j}(\omega) + \kappa_{M,j}(\omega)\right] U\left(x_j\right) = -\kappa_j(\omega)\, U\left(x_j\right) \tag{5}$$

for $j = 1, 2, \ldots .n$. Equation (4) is the damper equilibrium equation, where $N(x_j^+)$ and $N(x_j^-)$ are the axial forces to the right and left of the damper, respectively. Equation (5) is the damper constitutive equation, where symbols $\kappa_{G,j}(\omega)$ and $\kappa_{M,j}(\omega)$ are frequency-dependent stiffness parameters given as [42,43]:

$$\kappa_{G,j}(\omega) = k_{G,j} + \mathrm{i}\omega \cdot c_{G,j}; \quad \kappa_{M,j}(\omega) = \frac{\left(k_{M,j} + \mathrm{i}\omega \cdot c_{M,j}\right) M_j \omega^2}{M_j \omega^2 - \left(k_{M,j} + \mathrm{i}\omega \cdot c_{M,j}\right)}. \tag{6.1,2}$$

Equation (6.2), derived as explained in Refs. [42,43], shows that in the frequency domain attached mass dampers can be treated as grounded dampers, i.e. the (steady-state) reaction force of an attached mass damper depends on the displacement of the attachment point only through a pertinent frequency-dependent term, involving stiffness/damping/mass of the mass damper. Also, notice that a lumped mass along the bar can be modelled as a mass damper with $k_{M,j} = \infty$ in Eq. (6.2).

In Eq. (3), $\Delta U_j = U(x_j^+) - U(x_j^-)$ is the relative axial displacement between cross sections at $x = x_j^+$ and $x = x_j^-$, caused by the internal dampers to the left and right of $x = x_j$. It can be written as

$$\Delta U_j = \underbrace{U\left(x_j^+\right) - U\left(x_j\right)}_{\Delta U_j^+} + \underbrace{U\left(x_j\right) - U\left(x_j^-\right)}_{\Delta U_j^-} = \frac{N\left(x_j^+\right)}{\kappa_{\Delta U_j^+}(\omega)} + \frac{N\left(x_j^-\right)}{\kappa_{\Delta U_j^-}(\omega)} \tag{7}$$

where $\kappa_{\Delta U_j^\pm}(\omega)$ are frequency-dependent stiffness terms of the internal dampers at $x = x_j^+$ and $x = x_j^-$:

$$\kappa_{\Delta U_j^\pm}(\omega) = k_{\Delta U_j^\pm} + \mathrm{i}\omega \cdot c_{\Delta U_j^\pm}. \tag{8}$$

Next, let $\mathbf{Y}(x) = \left[U(x)\ N(x)\right]^T$ be the vector of frequency response variables solution to Eq. (1), and $\mathbf{\Lambda}_j = \left[R_j\ \Delta U_j\right]^T$ the vector collecting the unknown reaction force and relative axial displacement at $x = x_j$. From Eq. (1), $\mathbf{Y}(x)$ can be cast in the following general form, based on the linear superposition principle [44]:

$$\mathbf{Y}(x) = \mathbf{\Omega}(x)\,\mathbf{c} + \sum_{j=1}^{n} \mathbf{J}\left(x, x_j\right) \mathbf{\Lambda}_j + \mathbf{Y}^{(f)}(x). \tag{9}$$

In Eq. (9), $\mathbf{\Omega}(x)\,\mathbf{c}$ is the solution to the complementary (homogeneous) equation associated with Eq. (1); $\mathbf{J}\left(x, x_j\right)\mathbf{\Lambda}_j$ is the particular solution related to the unknown vector $\mathbf{\Lambda}_j$, while $\mathbf{Y}^{(f)}(x)$ is the particular solution attributable to the applied load $f(x)$. They can be represented as

$$\mathbf{\Omega}(x)\,\mathbf{c} = \begin{bmatrix} \Omega_{U1}(x) & \Omega_{U2}(x) \\ \Omega_{N1}(x) & \Omega_{N2}(x) \end{bmatrix} \begin{bmatrix} c_1 \\ c_2 \end{bmatrix} \tag{10}$$

with $\mathbf{c} = \left[c_1\ c_2\right]^T$ a vector of integration constants;

$$\mathbf{J}\left(x, x_j\right) = \left[\mathbf{J}^{(P)}\ \mathbf{J}^{(\Delta U)}\right] \qquad \mathbf{J}^{(P)} = \begin{bmatrix} J_U^{(P)} \\ J_N^{(P)} \end{bmatrix}; \qquad \mathbf{J}^{(\Delta U)} = \begin{bmatrix} J_U^{(\Delta U)} \\ J_N^{(\Delta U)} \end{bmatrix} \tag{11.1–3}$$

where superscripts (P) and (ΔU) denote the particular integrals associated with a unit axial force $P = 1$ and a unit relative displacement $\Delta U = 1$. Also, $\mathbf{Y}^{(f)}(x) = \left[U^{(f)}\ N^{(f)}\right]^T$ is given by

$$\mathbf{Y}^{(f)}(x) = \int_a^b \mathbf{J}^{(P)}(x, \xi)\, f(\xi)\, \mathrm{d}\xi. \tag{12}$$

All terms in Eq. (10) through Eq. (11) are available in a simple analytical form, which involve generalized functions [26]. Closed-form solutions are available also for Eq. (12) related to the applied load, following simple rules of integration for generalized functions. For brevity, mathematical derivations are reported in "Appendix 1".

At this stage, Eq. (9) for the frequency response vector involves the unknowns $\mathbf{\Lambda}_j$ at the dampers locations $x = x_j$, for $j = 1, 2, \ldots n$. The simple procedure explained in the following allows all unknowns $\mathbf{\Lambda}_j$ to be expressed in terms of the vector of integration constants $\mathbf{c}$. It is noted indeed that the following two conditions can be set at every dampers location $x = x_j$, based on Eqs. (4–5) for R_j, and Eq. (7) for ΔU_j:

$$R_j = -\kappa_j(\omega)\, U\left(x_j\right) = -\kappa_j(\omega)\left(U\left(x_j^-\right) + \frac{N\left(x_j^-\right)}{\kappa_{\Delta U_j^-}(\omega)}\right), \tag{13}$$

$$\begin{aligned}\Delta U_j &= \frac{N\left(x_j^-\right)}{\kappa_{\Delta U_j^-}(\omega)} + \frac{N\left(x_j^+\right)}{\kappa_{\Delta U_j^+}(\omega)} = N\left(x_j^-\right)\left(\frac{1}{\kappa_{\Delta U_j^-}(\omega)} + \frac{1}{\kappa_{\Delta U_j^+}(\omega)}\right) - \frac{R_j}{\kappa_{\Delta U_j^+}(\omega)} \\ &= N\left(x_j^-\right)\left(\frac{1}{\kappa_{\Delta U_j^-}(\omega)} + \frac{1}{\kappa_{\Delta U_j^+}(\omega)}\right) + \frac{\kappa_j(\omega)}{\kappa_{\Delta U_j^+}(\omega)}\left(U\left(x_j^-\right) + \frac{N\left(x_j^-\right)}{\kappa_{\Delta U_j^-}(\omega)}\right).\end{aligned} \tag{14}$$

Next, on replacing Eq. (9) for $U(x)$, $N(x)$ on the RHS of Eqs. (13–14), it can be noticed that $U(x_j^-)$, $N(x_j^-)$ involve only unknowns $\mathbf{\Lambda}_k$ for $k < j$. See, in this respect, that the particular solutions $J_U^{(P)}(x_j^-, x_k)$, $J_U^{(\Delta U)}(x_j^-, x_k)$, $J_N^{(P)}(x_j^-, x_k)$, $J_N^{(\Delta U)}(x_j^-, x_k)$, given by Eqs. (A.5–A.8) in "Appendix 1", are not zero only for $x_j^- > x_k$ and vanish for $x_j^- < x_k$. This makes it possible to cast vector $\mathbf{\Lambda}_1$ at the first dampers location x_1, and vectors $\mathbf{\Lambda}_j$ at dampers locations $x = x_j$, for $j = 2, \ldots, n$, in the following forms:

$$\mathbf{\Lambda}_1 = \mathbf{\Phi}_{\mathbf{\Omega}}(x_1)\,\mathbf{c} + \mathbf{\Phi}^{(f)}(x_1), \tag{15}$$

$$\mathbf{\Lambda}_j = \mathbf{\Phi}_{\mathbf{\Omega}}\left(x_j\right)\mathbf{c} + \sum_{k=1}^{j-1}\mathbf{\Phi}_{\mathbf{J}}\left(x_j^-, x_k\right)\mathbf{\Lambda}_k + \mathbf{\Phi}^{(f)}\left(x_j\right) \quad \text{for } j = 2, \ldots, n \tag{16}$$

where symbols are as follows: $\mathbf{\Phi}_{\mathbf{\Omega}}\left(x_j\right)$ is the 2×2 matrix

$$\mathbf{\Phi}_{\mathbf{\Omega}}\left(x_j\right) = \begin{bmatrix} -\kappa_j(\omega)\left(\left(\mathbf{\Omega}\left(x_j\right)\right)_1 + \frac{(\mathbf{\Omega}(x_j))_2}{\kappa_{\Delta U_j^-}(\omega)}\right) \\ \left(\frac{1}{\kappa_{\Delta U_j^-}(\omega)} + \frac{1}{\kappa_{\Delta U_j^+}(\omega)}\right)\left(\mathbf{\Omega}\left(x_j\right)\right)_2 + \frac{\kappa_j(\omega)}{\kappa_{\Delta U_j^+}(\omega)}\left(\left(\mathbf{\Omega}\left(x_j\right)\right)_1 + \frac{(\mathbf{\Omega}(x_j))_2}{\kappa_{\Delta U_j^-}(\omega)}\right) \end{bmatrix} \tag{17}$$

being $(\mathbf{\Omega}(x_j))_i$ row vectors coinciding with the ith row of matrix $\mathbf{\Omega}(x_j)$; further, $\mathbf{\Phi}_{\mathbf{J}}\left(x_j^-, x_k\right)$, for $k < j$, is the 2×2 matrix

$$\mathbf{\Phi}_{\mathbf{J}}\left(x_j^-, x_k\right) = \begin{bmatrix} -\kappa_j(\omega)\left(\left(\mathbf{J}\left(x_j^-, x_k\right)\right)_1 + \frac{\left(\mathbf{J}\left(x_j^-, x_k\right)\right)_2}{\kappa_{\Delta U_j^-}(\omega)}\right) \\ \left(\frac{1}{\kappa_{\Delta U_j^-}(\omega)} + \frac{1}{\kappa_{\Delta U_j^+}(\omega)}\right)\left(\mathbf{J}\left(x_j^-, x_k\right)\right)_2 + \frac{\kappa_j(\omega)}{\kappa_{\Delta U_j^+}(\omega)}\left(\left(\mathbf{J}\left(x_j^-, x_k\right)\right)_1 + \frac{\left(\mathbf{J}\left(x_j^-, x_k\right)\right)_2}{\kappa_{\Delta U_j^-}(\omega)}\right) \end{bmatrix} \tag{18}$$

where $(\mathbf{J}(x_j^-, x_k))_i$ are the row vectors coinciding with the ith row of matrix $\mathbf{J}\left(x_j^-, x_k\right)$, and $\mathbf{\Phi}^{(f)}(x_j)$ is the 2×1 vector

Table 1 Sets $\mathbb{N}_q^{(j)}$ in Eq. (20) for $n = 4$ dampers locations

	$j = 2$	$j = 3$	$j = 4$
$q = 2$	$\mathbb{N}_2^{(2)} = \{(2, 1)\}$	$\mathbb{N}_2^{(3)} = \{(3, 1), (3, 2)\}$	$\mathbb{N}_2^{(4)} = \{(4, 1), (4, 2), (4, 3)\}$
$q = 3$	–	$\mathbb{N}_3^{(3)} = \{(3, 2, 1)\}$	$\mathbb{N}_3^{(4)} = \{(4, 3, 2), (4, 3, 1), (4, 2, 1)\}$
$q = 4$	–	–	$\mathbb{N}_4^{(4)} = \{(4, 3, 2, 1)\}$

$$\mathbf{\Phi}^{(f)}(x_j) = \begin{bmatrix} -\kappa_j(\omega)\left(U^{(f)}(x_j) + \frac{N^{(f)}(x_j)}{\kappa_{\Delta U_j^-}(\omega)}\right) \\ \left(\frac{1}{\kappa_{\Delta U_j^-}(\omega)} + \frac{1}{\kappa_{\Delta U_j^+}(\omega)}\right) N^{(f)}(x_j) + \frac{\kappa_j(\omega)}{\kappa_{\Delta U_j^+}(\omega)}\left(U^{(f)}(x_j) + \frac{N^{(f)}(x_j)}{\kappa_{\Delta U_j^-}(\omega)}\right) \end{bmatrix}. \tag{19}$$

Notice the formal correspondence between the rows of $\mathbf{\Phi_\Omega}(x_j)$, $\mathbf{\Phi_J}\left(x_j^-, x_k\right)$, $\mathbf{\Phi}^{(f)}(x_j)$ and Eqs. (13–14).

Equations (15–16) for $\mathbf{\Lambda}_j$ serve as a basis to obtain $\mathbf{\Lambda}_j$ as a function of the vector of integration constants $\mathbf{c}$ only. Indeed, starting from Eq. (15) for $\mathbf{\Lambda}_1$, Eq. (16) leads to the following general form of $\mathbf{\Lambda}_j$:

$$\mathbf{\Lambda}_j = \mathbf{\Phi_\Omega}(x_j)\mathbf{c} + \mathbf{\Phi}^{(f)}(x_j) + \sum_{2\le q\le j} \sum_{(\underbrace{j, l, m, \ldots, r, s}_{q})\in \mathbb{N}_q^{(j)}} \mathbf{\Phi_J}\left(x_j^-, x_l\right) \mathbf{\Phi_J}\left(x_l^-, x_m\right) \cdots \mathbf{\Phi_J}\left(x_r^-, x_s\right) \times \left(\mathbf{\Phi_\Omega}(x_s)\mathbf{c} + \mathbf{\Phi}^{(f)}(x_s)\right) \tag{20}$$

where $\mathbb{N}_q^{(j)} = \{(\underbrace{j, l, m, \ldots r, s}_{q}) : j > l > m > \cdots > r > s; l, m, \ldots r, s = 1, 2, \ldots, (j-1)\}$ is the set including all possible q-ples of indices $(\underbrace{j, l, m, \ldots r, s}_{q})$ such that $j > l > m > \cdots > r > s$, being $2 \le q \le j$. For instance, with $n = 4$ dampers locations the following sets shall be considered in Eq. (20) (Table 1):

Finally, on replacing Eq. (20) for $\mathbf{\Lambda}_j$ in Eq. (9), the following relation is derived for the vector $\mathbf{Y}(x)$ of response variables:

$$\mathbf{Y}(x) = \tilde{\mathbf{Y}}(x)\,\mathbf{c} + \tilde{\mathbf{Y}}^{(f)}(x) \tag{21}$$

where the only unknown is the vector of integration constants $\mathbf{c}$, while $\tilde{\mathbf{Y}}(x)$ and $\tilde{\mathbf{Y}}^{(f)}(x)$ are given as

$$\tilde{\mathbf{Y}}(x) = \mathbf{\Omega}(x) + \sum_{j=1}^{n} \mathbf{J}\left(x, x_j\right) \mathbf{\Phi_\Omega}\left(x_j\right) + \sum_{j=2}^{n} \mathbf{J}\left(x, x_j\right) \left\{ \sum_{2\le q\le j} \sum_{(\underbrace{j, l, m, \ldots, r, s}_{q})\in \mathbb{N}_q^{(j)}} \mathbf{\Phi_J}\left(x_j^-, x_l\right) \mathbf{\Phi_J}\left(x_l^-, x_m\right) \cdots \mathbf{\Phi_J}\left(x_r^-, x_s\right) \mathbf{\Phi_\Omega}(x_s) \right\}, \tag{22}$$

$$\tilde{\mathbf{Y}}^{(f)}(x) = \mathbf{Y}^{(f)}(x) + \sum_{j=1}^{n} \mathbf{J}\left(x, x_j\right) \mathbf{\Phi}^{(f)}\left(x_j\right) + \sum_{j=2}^{n} \mathbf{J}\left(x, x_j\right) \left\{ \sum_{2\le q\le j} \sum_{(\underbrace{j, l, m, \ldots, r, s}_{q})\in \mathbb{N}_q^{(j)}} \mathbf{\Phi_J}\left(x_j^-, x_l\right) \mathbf{\Phi_J}\left(x_l^-, x_m\right) \cdots \mathbf{\Phi_J}\left(x_r^-, x_s\right) \mathbf{\Phi}^{(f)}(x_s) \right\}. \tag{23}$$

In Eq. (22), $\tilde{\mathbf{Y}}(x)$ depends on the bar parameters only, through matrices $\mathbf{\Omega}(x)$ and $\mathbf{J}\left(x, x_j\right)$ (see also Eq. (17) for $\mathbf{\Phi_\Omega}\left(x_j\right)$ and Eq. (18) for $\mathbf{\Phi_J}(x_j^-, x_k)$), while in Eq. (23) $\tilde{\mathbf{Y}}^{(f)}(x)$ depends on the bar parameters and

applied load, as includes the particular integral $\mathbf{Y}^{(f)}(x)$ and the load-dependent vectors $\mathbf{\Phi}^{(f)}\left(x_j\right)$. Notice that Eq. (20) through Eq. (23) mirror those obtained in Ref. [35] for the bending response of beams with multiple dampers at the same position. Next, two further steps have to be made, to derive closed-form expressions for the frequency response vector $\mathbf{Y}(x)$ in Eq. (21).

Firstly, consider the integration constants $\mathbf{c}$ in Eq. (21). Enforcing the B.C. of the bar leads to 2 equations, regardless of the number of dampers, with general form

$$\mathbf{Bc} = \mathbf{r} \rightarrow \mathbf{c} = \mathbf{B}^{-1}\mathbf{r} \tag{24}$$

where vector $\mathbf{r}$ involves the load-dependent terms $\tilde{\mathbf{Y}}^{(f)}(x)$ in Eq. (23), as computed at the bar ends. The 2×2 matrix $\mathbf{B}$ can readily be inverted in a symbolic form [26]. Therefore, from Eq. (24) closed-form expressions can be derived for $\mathbf{c}$, to be replaced in Eq. (21).

Secondly, with regard to the particular integrals $\mathbf{Y}^{(f)}(x)$ involved in Eq. (23), it is noticed that every integral in Eq. (12) can be reverted to the general form $\int_a^b g(\xi)\, H(x-\xi)\, d\xi$, with $g(x)$ given by the product of the loading function and certain trigonometric functions, see the analytical expressions of $\mathbf{J}^{(P)}(x, x_0)$ in "Appendix 1". For such integrals, closed-form expressions can readily be derived when, for instance, the loading functions have a polynomial form, as generally encountered in engineering applications. Details may be found in Ref. [45] and are briefly recalled in "Appendix 1".

It may be concluded that Eq. (21) provides closed-form expressions of the frequency response of the bar with any number of dampers, under arbitrarily placed point/polynomial loads.

3.1 Remarks

The first remark is that Eq. (24) can be used for both homogeneous and non-homogeneous B.C., the latter as due to end dampers. In fact, the B.C. can still be considered as homogeneous, while the end dampers are modelled as internal dampers located at $x_1 = 0^+$ and $x_n = L^-$ [45].

Free vibration solution can readily be obtained from Eq. (24) with $\mathbf{r} = \mathbf{0}$. The characteristic equation $Det\left(\mathbf{B}(\omega)\right) = 0$ provides the eigenvalues, and corresponding eigenfunctions are given by Eq. (21) with load-dependent term $\tilde{\mathbf{Y}}^{(f)}(x) = \mathbf{0}$.

Changes to consider a single damper at a given position are straightforward. If no external damper occurs at $x = x_j$, $\kappa_j(\omega) = 0$ shall be set at $x = x_j$. This will automatically set equal to zero the first row in matrices $\mathbf{\Phi_\Omega}\left(x_j\right)$, $\mathbf{\Phi_J}\left(x_j^-, x_k\right)$ and $\mathbf{\Phi}^{(f)}\left(x_j\right)$. Being $R_j = 0$ at $x = x_j$, the first column of matrix $\mathbf{\Phi_J}\left(x_m^-, x_j\right)$ shall be set equal to zero for all $x_m^- > x_j$. Obviously, if at $x = x_j$ there is no external damper but there is an internal damper, $N\left(x_j^-\right) = N\left(x_j^+\right)$, and, in view of Eq. (7), $\kappa_{\Delta U_j^+}(\omega) = \kappa_{\Delta U_j^-}(\omega) = \kappa_{\Delta U_j}(\omega)/2$, with $\kappa_{\Delta U_j}(\omega)$ the frequency-dependent stiffness of the internal damper at $x = x_j$. If no internal damper occurs at $x = x_j$, $\kappa_{\Delta U_j^+}(\omega) = \kappa_{\Delta U_j^-}(\omega) = \infty$ shall be set at $x = x_j$. As a result, the second row of matrices $\mathbf{\Phi_\Omega}\left(x_j\right)$, $\mathbf{\Phi_J}\left(x_j^-, x_k\right)$, and $\mathbf{\Phi}^{(f)}\left(x_j\right)$ will be equal to zero. Also, being $\Delta U_j = 0$ at $x = x_j$, the second column of matrix $\mathbf{\Phi_J}\left(x_m^-, x_j\right)$ shall be set equal to zero for all $x_m^- > x_j$.

An important remark concerns the case in which the applied load is a point force at $x = x_0$, i.e. $f(x) = P \cdot \delta(x - x_0)$. In this case, Eq. (12) yields $\mathbf{Y}^{(f)}(x) = P \cdot \mathbf{J}^{(P)}(x, x_0)$. If, in particular, the point force $P \cdot \delta(x - x_0)$ is applied at a dampers location x_j, i.e. $x_0 = x_j$, Eq. (7) will be written as $R_j + P + N(x_j^+) = N(x_j^-)$, and, consequently, an additional term $-P/\kappa_{\Delta U_j^+}(\omega)$ shall be considered on the RHS of Eq. (14) and in the second entry of vector $\mathbf{\Phi}^{(f)}\left(x_j\right)$ given by Eq. (19) where, in this case, $N^{(f)}(x)$ will be computed at $x = x_j^-$.

At this stage, a few comments are in order on the advantages of the proposed method. Equation (21) is an exact closed-form expression of the FRFs, for all response variables. It fulfils axial force and axial displacement discontinuities at the locations of dampers and point load (see "Appendix 1"). Equation (21) can readily be implemented for any number and positions of dampers, and positions of point/distributed loads relative to the dampers, with no changes, whereas number and positions of dampers or load vary along the bar. These are significant advantages over the classical exact approach, where the vibration response in every bar segment, either between two consecutive positions of dampers/point load or under a distributed load, is represented in terms of two integration constants, totalling $2 \times k$ constants for k segments. These integration constants have to be computed by a set of equations, which is built by enforcing the B.C. and matching conditions between

the responses over contiguous bar segments. By this approach, the coefficient matrix associated with the set of equations to be solved has to be updated whenever the positions of dampers or load change along the axis, and its size increases with the number of dampers. Also, it has to be re-inverted for any forcing frequency of the applied load.

The exact closed-form expressions (21) can serve as benchmark for FRFs built by a standard FE method with two-node truss elements. Further advantages are that, in a standard FE method, a mesh node shall be inserted at the application point of any damper or point load, and re-meshing may be required whenever dampers or loads change position.

4 Dynamic stiffness matrix and load vector

Consider the bar in Fig. 1, carrying an arbitrary number of multiple dampers at the same position and subjected to arbitrary loads. Let $\mathbf{u} = \left[U_1 \; U_2 \right]^T$ and $\mathbf{f} = \left[H_1 \; H_2 \right]^T$ be the vectors collecting nodal displacements and forces; $U_1 = U(0)$ and $U_2 = U(L)$, and, in view of the positive sign conventions for nodal forces and internal stress resultants:

$$H_1 = -N(0), \quad H_2 = N(L). \tag{25}$$

The following nodal equation holds [4]:

$$\mathbf{f} = \mathbf{D}(\omega)\,\mathbf{u} + \mathbf{f}_0 \tag{26}$$

where $\mathbf{D}(\omega)$ is the dynamic stiffness matrix and $\mathbf{f}_0$ is the nodal force vector attributable to the loads acting along the bar. Elements of both matrix $\mathbf{D}(\omega)$ and vector $\mathbf{f}_0$ can be derived based on the FRFs (21), as follows.

Let $\mathbf{G}^{(U)}(x, x_0) = \left[U^{(U)} \; N^{(U)} \right]^T$ be the frequency response vector of the bar, subjected to harmonic axial displacement $U \cdot e^{\mathrm{i}\omega t}$, for $U = 1$, applied at the ends $x_0 = 0$ or $x_0 = L$. It may be seen that $\mathbf{G}^{(U)}(x, x_0)$ takes the form (21) with no load-dependent terms $\tilde{\mathbf{Y}}^{(f)}(x)$, i.e.

$$\mathbf{G}^{(U)}(x, x_0) = \tilde{\mathbf{Y}}(x)\,\mathbf{c}^{(U)} \text{ for } \mathbf{c}^{(U)} = \mathbf{B}^{-1}\mathbf{e}^{(U)}. \tag{27.1,2}$$

In Eq. (27.2), matrix $\mathbf{B}$ is

$$\mathbf{B} = \begin{bmatrix} \left(\tilde{\mathbf{Y}}(0)\right)_{1,1} & \left(\tilde{\mathbf{Y}}(0)\right)_{1,2} \\ \left(\tilde{\mathbf{Y}}(L)\right)_{1,1} & \left(\tilde{\mathbf{Y}}(L)\right)_{1,2} \end{bmatrix} \tag{28}$$

where $\left(\tilde{\mathbf{Y}}(\cdot)\right)_{m,n}$ is the m,n element of matrix $\tilde{\mathbf{Y}}(x)$ given by Eq. (22), while vector $\mathbf{e}^{(U)}$ is

$$\begin{aligned} \mathbf{e}^{(U)} &= \left[1 \; 0 \right]^T \quad \text{if } x_0 = 0, \\ \mathbf{e}^{(U)} &= \left[0 \; 1 \right]^T \quad \text{if } x_0 = L. \end{aligned} \tag{29.1,2}$$

At this stage, the elements of matrix $\mathbf{D}(\omega)$ can be built based on Eq. (27.1). In particular, bearing in mind that the elements of matrix $\mathbf{D}(\omega)$ are the nodal forces due to unit displacements/rotations at the nodes, and taking into account relations (25) between nodal forces and stress resultants, it yields

$$\mathbf{D}(\omega) = \begin{bmatrix} -N^{(U)}(0, 0) & -N^{(U)}(0, L) \\ N^{(U)}(L, 0) & N^{(U)}(L, L) \end{bmatrix} \tag{30}$$

where $N^{(U)}(x, x_0)$ is given by Eq. (27.1) with $x = 0, L$ and $x_0 = 0, L$. Notice that all elements in Eq. (30) for $\mathbf{D}(\omega)$ are readily available in a closed form, as Eq. (27.1) provides closed-form expressions for $\mathbf{G}^{(U)}(x, x_0)$ (see Sect. 2).

Next, denote by $\mathbf{Y}_0(x) = \left[U_0 \; N_0 \right]^T$ the frequency response vector (21) of the bar in Fig. 1 under load $f(x)$, when both ends are fixed. Let $\mathbf{c}^{(f)}$ be the vector of integration constants in Eq. (21) where, in this case, superscript (f) distinguishes vectors $\mathbf{c}^{(f)}$ from vectors $\mathbf{c}^{(U)}$ associated with unit displacement at the bar ends. They are computed by the following equations:

$$\mathbf{B}\mathbf{c}^{(f)} = \mathbf{e}^{(f)} \quad \mathbf{e}^{(f)} = \left[-\tilde{U}^{(f)}(0) \; -\tilde{U}^{(f)}(L) \right]^T \tag{31}$$

where $\tilde{U}^{(f)}$ is taken from $\tilde{\mathbf{Y}}^{(f)}(x) = \left[\tilde{U}^{(f)} \; \tilde{N}^{(f)} \right]^T$ in Eq. (23). On using $\mathbf{c}^{(f)}$ in the closed-form expressions (21), and in view of relations (25), the exact load vector is then given in the closed form

$$\mathbf{f}_0 = \left[-N_0(0) \;\; N_0(L) \right]^T . \tag{32}$$

Exact matrix (30) and vector (32) can be assembled into the global dynamic stiffness matrix and load vector of a 2D truss structure, by a standard finite element procedure. It is interesting to note that matrix (30) and vector (32) hold the same size for any number of dampers and loads. For this reason, the size of the corresponding global dynamic stiffness matrix and load vector will depend only on the number of nodes, regardless of the number of dampers and loads.

Upon deriving the global nodal solution, the exact frequency response can be built in every truss member, using the following expression:

$$\mathbf{Y}(x) = \mathbf{G}^{(U)}(x, 0)\, U_1 + \mathbf{G}^{(U)}(x, L)\, U_2 + \mathbf{Y}_0(x) \tag{33}$$

where U_i are the nodal displacements in vector $\mathbf{u}$, while $\mathbf{Y}_0(x)$ is the frequency response of the bar to the applied loads, when both ends are fixed.

At this stage, a few remarks are in order. The exact dynamic stiffness matrix (30) and load vector (32) can be derived by an alternative procedure, proposed in Refs. [26,35] and briefly recalled in "Appendix 2", for brevity. Although the two approaches both lead to the exact dynamic stiffness matrix and load vector in a symbolic form, there is a relevant difference between the two approaches. Once the global dynamic stiffness matrix of the truss structure is built and the nodal displacements $\mathbf{u}$ are computed, the approach in Refs. [26,35] would require back-calculating the vector of integration constants $\mathbf{c} = \left[c_1 \;\; c_2 \right]^T$, see Eq. (B.8) in "Appendix 2", to be used in Eq. (21) to compute the frequency response vector along each member. On the contrary, Eq. (33) is expressed directly in terms of nodal displacements $\mathbf{u}$. This provides an immediate insight into how the response variables along any member are affected by nodal displacements and loads, with relevant advantages in terms of computational effort.

A final remark is that the approach described above can readily be extended to build exact dynamic stiffness matrix and load vector for the bending response of Euler–Bernoulli beams with multiple dampers at the same position, as alternative to that devised in Ref. [35]. This is left for further development.

5 Numerical application

Consider the bar in Fig. 2, with parameters: $L = 15$ m, $EA = 1.255 \times 10^9$ N, $m_0 = 49.54$ kgm^{-1} (corresponding to Young's modulus $= 19.5 \times 10^{10}$ Nm^{-2}, cross section area $= 64.34 \times 10^{-4}$ m^2, mass density $= 7.7 \times 10^3$ kgm^{-3}). The bar carries two external mass dampers at $x = L/3$ and $x = 2L/3$. There are two internal dampers to the right and left of each mass damper, modelling imperfect internal connections. In addition, two axial dampers are located at the two ends. Parameters are reported in Table 2.

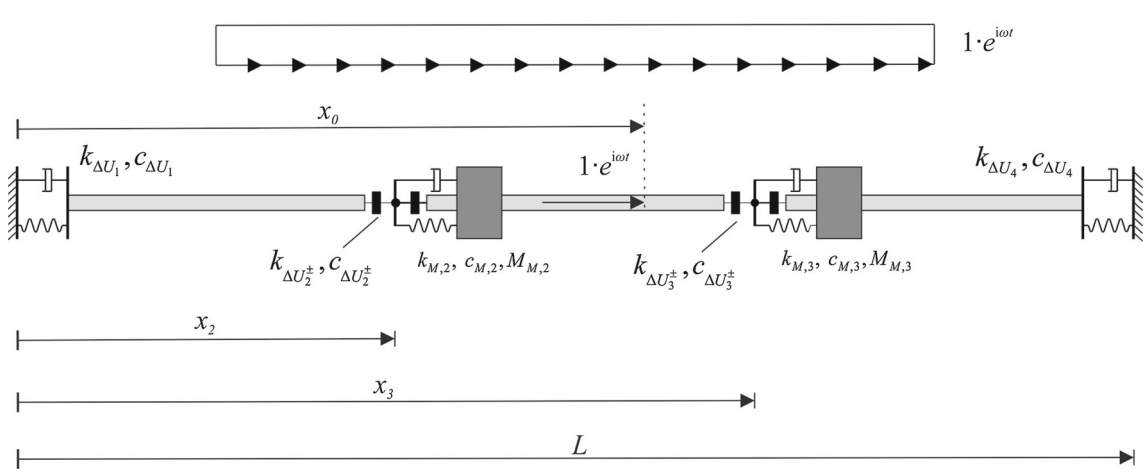

Fig. 2 Bar with multiple dampers at $x_2 = L/3$, $x_3 = 2L/3$, and single dampers at the two ends, under: **a** point load $1 \cdot e^{i\omega t}$ at $x = x_0$; **b** uniformly distributed load $f(x, t) = 1 \cdot e^{i\omega t}$ over $[L/6, 5L/6]$

Table 2 Bar in Fig. 2: spring stiffness and damping coefficients of dampers

Damper	Spring stiffness (Nm^{-1})	Damping coefficient ($\mathrm{Nm}^{-1}\mathrm{s}$)
End damper at $x_1 = 0^+$	$k_{\Delta U_1} = 1 \times 10^7$	$c_{\Delta U_1} = 1 \times 10^3$
Mass damper at $x_2 = L/3 (M_2 = 400\ \mathrm{kg})$	$k_{M,2} = 1 \times 10^7$	$c_{M,2} = 1 \times 10^4$
Internal damper at $x_2^- = (L/3)^-$	$k_{\Delta U_2^-} = 5 \times 10^9$	$c_{\Delta U_2^-} = 1 \times 10^3$
Internal damper at $x_2^+ = (L/3)^+$	$k_{\Delta U_2^+} = 5 \times 10^9$	$c_{\Delta U_2^+} = 1 \times 10^3$
Mass damper at $x_3 = 2L/3\ (M_3 = 400\ \mathrm{kg})$	$k_{M,3} = 1 \times 10^7$	$c_{M,3} = 1 \times 10^4$
Internal damper at $x_3^- = (2L/3)^-$	$k_{\Delta U_3^-} = 1 \times 10^9$	$c_{\Delta U_3^-} = 1 \times 10^3$
Internal damper at $x_3^- = (2L/3)^-$	$k_{\Delta U_3^+} = 1 \times 10^9$	$c_{\Delta U_3^+} = 1 \times 10^3$
End damper at $x_4 = L^-$	$k_{\Delta U_4} = 1 \times 10^7$	$c_{\Delta U_4} = 1 \times 10^3$

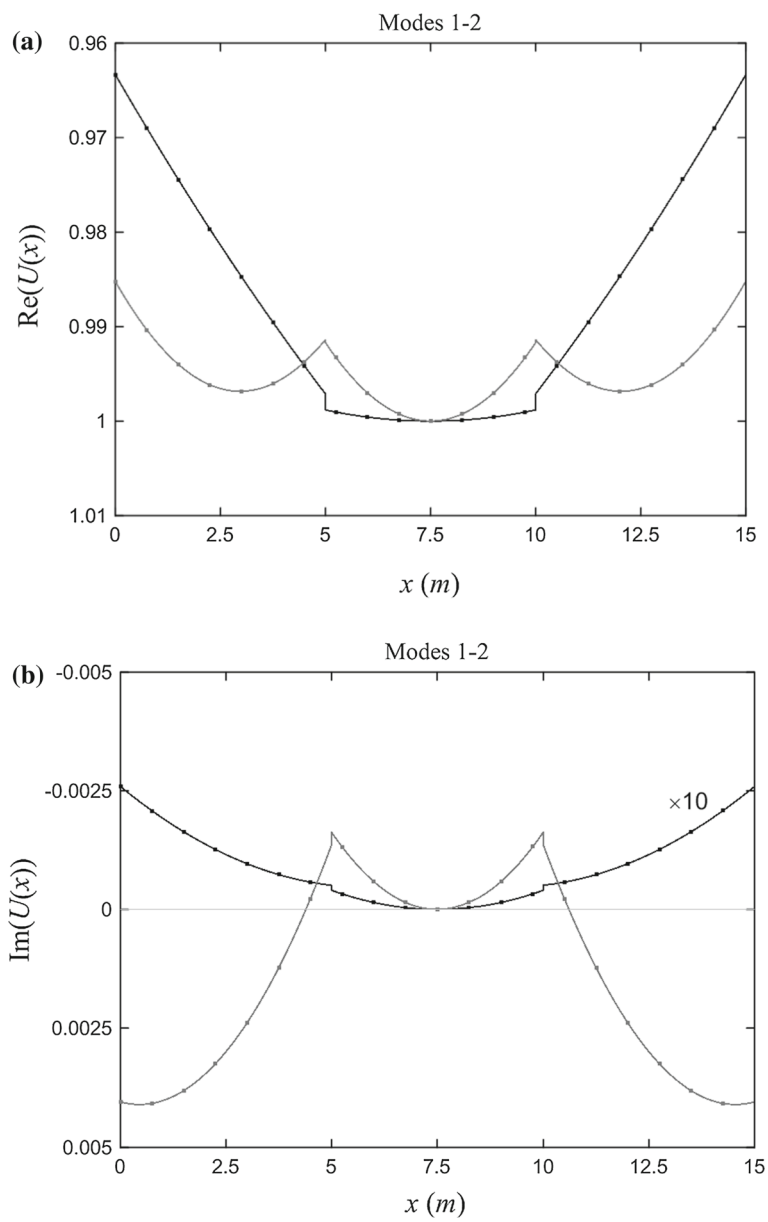

Fig. 3 Eigenfunctions of modes 1–2 of the bar in Fig. 2: **a** real part; **b** imaginary part

Free and forced axial vibrations under loading conditions in Fig. 2 are investigated via proposed and classical methods. The proposed method is implemented assuming homogeneous B.C. and modelling the end dampers as internal dampers at $x = 0^+$ and $x = L^-$. That is, a total number $n = 4$ of dampers locations is considered, $x_1 = 0^+, x_2 = L/3, x_3 = 2L/3, x_4 = L^-$. The classical method is implemented representing the vibration response in a trigonometric form with 2 integration constants over every segment between two consecutive positions of dampers/point load or under the uniform load, and enforcing matching conditions at the subdivision points along with the B.C. For the bar segment under the uniform load, a particular integral can be obtained in a closed form [46]. Both methods provide the exact responses. However, by the proposed method closed-form solutions are available using Eq. (21), while the classical solution involves up to $2 \times 5 = 10$ integration constants for the case of uniform load over $[L/6, 5L/6]$, to be computed numerically by inverting the coefficient matrix associated with the matching conditions + 2 B.C, for any forcing frequency of interest. Analogous comments hold for the free vibration response, as built by proposed and classical methods.

For a preliminary insight, Fig. 3 shows the axial displacement eigenfunctions of the first two modes, with corresponding eigenvalues in Table 3, as obtained from Eq. (21) with load-dependent term $\tilde{\mathbf{Y}}^{(f)}(x) = \mathbf{0}$

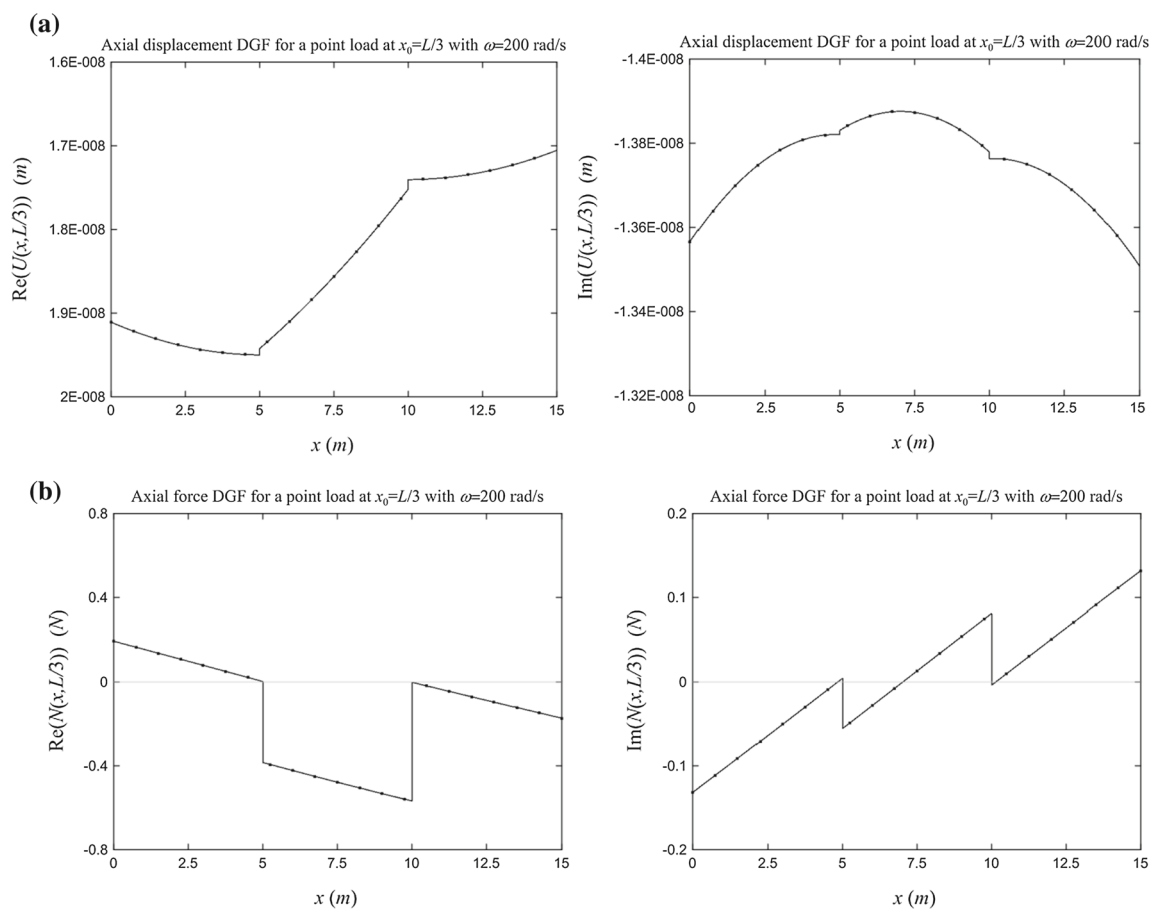

Fig. 4 Dynamic Green's functions of the bar in Fig. 2 for a point load with forcing frequency $\omega = 200$ rad/s, applied at $x_0 = L/3$: **a** axial displacement; **b** axial force; *left column* real part; *right column* imaginary part

Table 3 Eigenvalues and damping ratios of the first two modes of bar in Fig. 2

	Eigenvalue	Damping ratio
Mode 1	±97.645 +1.67142 i	0.0171148
Mode 2	±260.744 + 25.3886 i	0.0969117

(continuous line), and classical method (symbol "•"). Real and imaginary parts of the two solutions are in perfect agreement. The proposed solutions fulfil all required conditions at the dampers locations: axial displacement and force are discontinuous at $x_2 = L/3$, $x_3 = 2L/3$, while the axial displacement is not zero at $x_1 = 0^+$, $x_4 = L^-$. In particular, Fig. 3 shows the axial displacement to the right and left of x_2 and x_3,

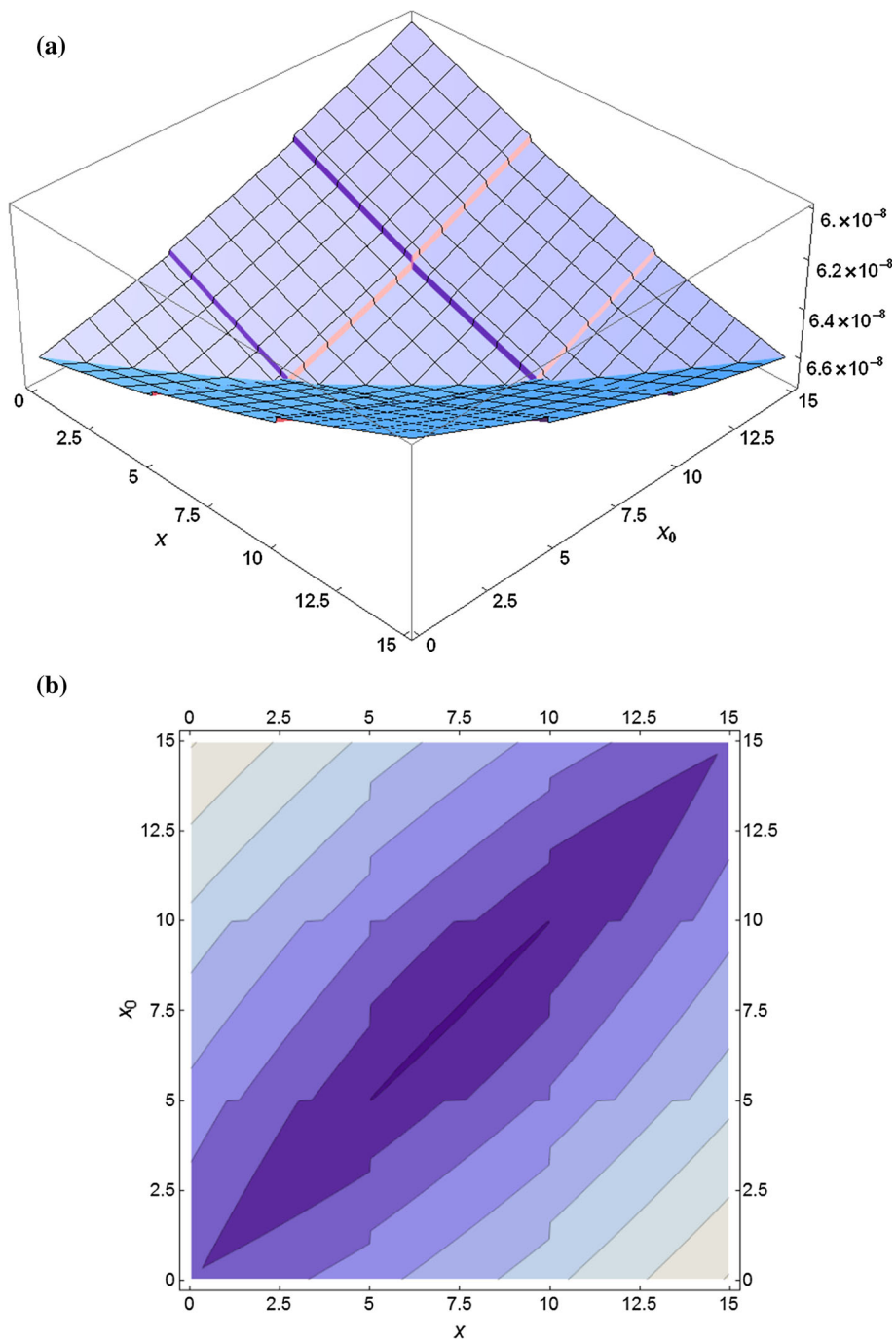

Fig. 5 Axial displacement dynamic Green's function of the bar in Fig. 2 for a point load with forcing frequency $\omega = 50$ rad/s, computed at x for various load positions x_0: **a** real part; **b** contour plot of real part

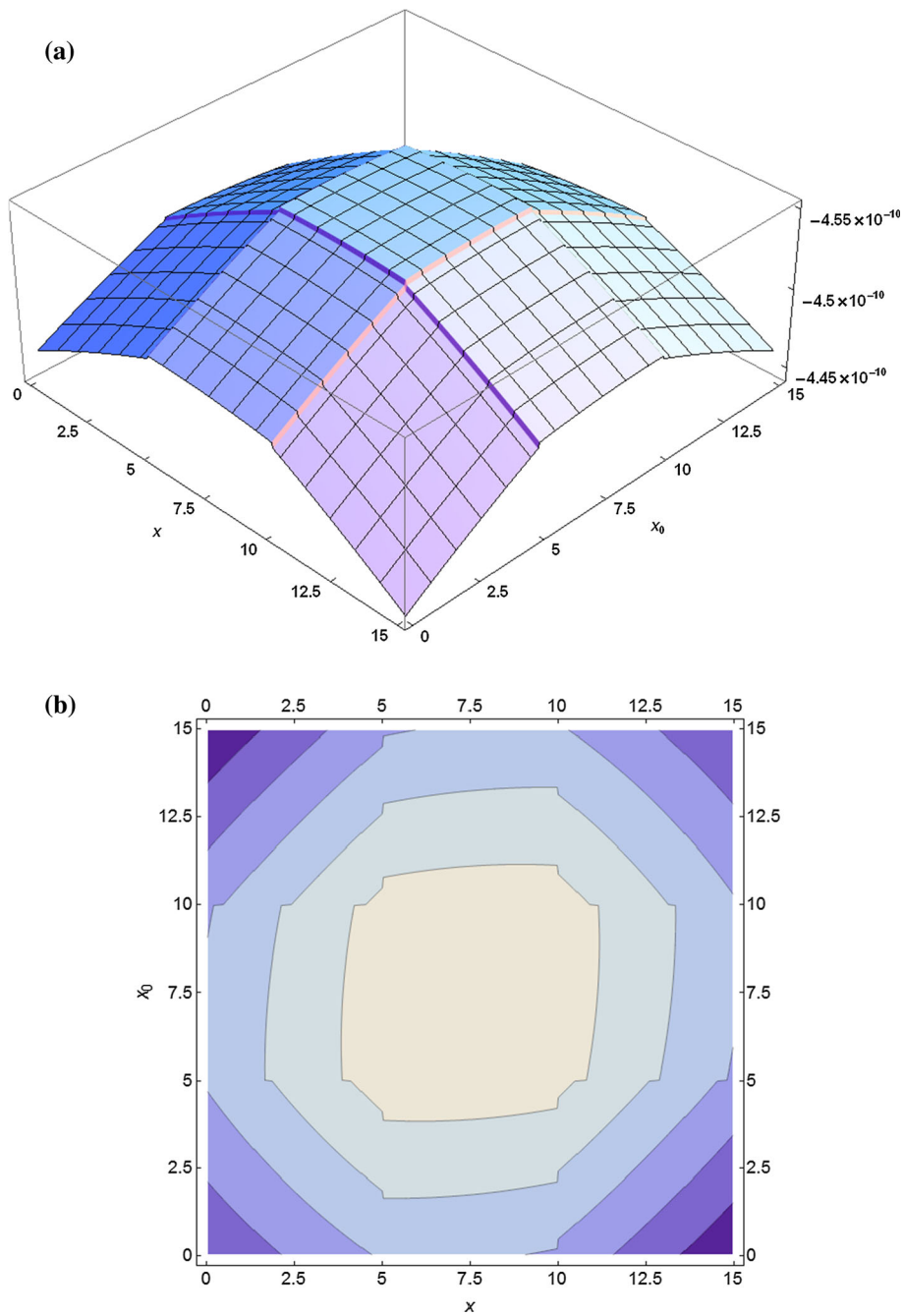

Fig. 6 Axial displacement dynamic Green's function of the bar in Fig. 2 for a point load with forcing frequency $\omega = 50$ rad/s, computed at x for various load positions x_0: **a** imaginary part; **b** contour plot of imaginary part

i.e. at $x_2^{\pm}$ and $x_3^{\pm}$. The axial displacement at $x = x_2$ and $x = x_3$, i.e. at the application points of the external mass dampers, can readily be computed using the constitutive equations of the internal dampers to the right of $x = x_2$ and $x = x_3$ (alternatively, those of the internal dampers to the left of $x = x_2$ and $x = x_3$ could be used):

$$U\left(x_j^+\right) - U\left(x_j\right) = \frac{N\left(x_j^+\right)}{\kappa_{\Delta U_j^+}(\omega)} \rightarrow U\left(x_j\right) = U\left(x_j^+\right) - \frac{N\left(x_j^+\right)}{\kappa_{\Delta U_j^+}(\omega)}. \tag{34}$$

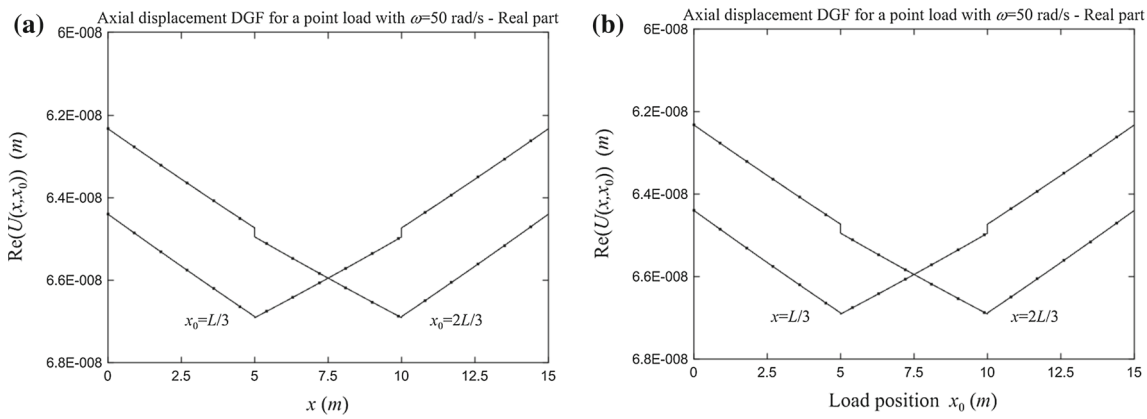

Fig. 7 Real part of axial displacement dynamic Green's function of the bar in Fig. 2 for a point load with forcing frequency $\omega = 50$ rad/s, computed at: **a** varying x for given load position x_0; **b** given x for varying load position x_0

Likewise, the displacement Z_j of the attached mass damper can be computed in terms of $U(x_j)$ as

$$Z_j = \frac{\left(k_{M,j} + \mathrm{i}\omega \cdot c_{M,j}\right) - M_j\omega^2}{\left(k_{M,j} + \mathrm{i}\omega \cdot c_{M,j}\right)} U\left(x_j\right). \tag{35}$$

Figure 4 shows the axial displacement and axial force DGFs for a point load $1 \cdot \mathrm{e}^{i\omega t}$ applied at $x_0 = L/3$ with forcing frequency $\omega = 200$ rad/sec, as obtained by Eq. (21) (continuous line) and the classical method (symbol "•"). Again, real and imaginary parts of the two solutions are in perfect agreement. As in Fig. 3, Fig. 4 shows the axial displacements at $x_2^{\pm}$ and $x_3^{\pm}$, and Eq. (34) can be used to compute the axial displacements at $x = x_2$ and $x = x_3$.

Figures 5 and 6 show real and imaginary parts of the axial displacement DGFs over the whole axis, computed by Eq. (21), for a point load $1 \cdot \mathrm{e}^{\mathrm{i}\omega t}$ applied at x_0 spanning $[0, L]$, with forcing frequency $\omega = 50$ rad/s. As expected [47], the DGF is symmetric, i.e. $U(x, x_0) = U(x_0, x)$. For a further insight into Figs. 5 and 6, Fig. 7 illustrates the real part of the axial displacement DGF, computed at varying x for given load position x_0, and vice-versa, as computed by Eq. (21) and the classical method. Obviously, axial displacements at $x = L/3$ and $x = 2L/3$ are computed using Eq. (34). The results in Fig. 7a, b are coincident, due to the symmetry of the DGF. Again, notice that exact proposed and exact classical solutions coincide.

Figure 8 shows the axial displacement of the mass damper at $x = L/3$, and the axial displacement at midspan, for a point load with varying excitation frequency ω and position x_0 along the bar, as computed by the proposed method. The contribution of the first mode is always dominating, regardless of the load position. The contribution of the second mode varies depending on load position and is almost negligible in the mass damper displacement.

Finally, Fig. 9 shows the axial displacement FRF at midspan for a uniform load over $[L/6, 5L/6]$ with $\omega = 50$ rad/s and $\omega = 100$ rad/s, for varying damping coefficients of the end dampers and mass dampers. It is apparent that the damping coefficient of the end dampers affects the response much more than that of the mass dampers.

All results obtained by the exact proposed method, shown in Figs. 8 and 9, have been compared with those obtained by the exact classical method, and a perfect agreement has always been encountered. It is noted, however, that the proposed method is more efficient and particularly suitable for constructing data in Figs. 8 and 9, because Eq. (21) for the frequency response function holds, in a closed form, for any position of the load relative to the dampers, with significant advantages in terms of implementation and computational effort. By the classical approach, instead, data in Fig. 8 are obtained by updating the coefficient matrix associated with the equations to be solved, depending on the position of the load relative to the dampers; also, the coefficient matrix has to be inverted numerically for any forcing frequency ω in Fig. 8 and set of damping values in Fig. 9. For brevity and clarity of presentation, results obtained by the classical method have not been included.

For completeness, Table 4 reports the elements of the exact dynamic stiffness matrix and load vector under uniform load in Fig. 2 with $\omega = 60$ rad/sec, computed by Eqs. (30–32) in Sect. 4 and Eqs. (B.6–B.7) in "Appendix 2". The two solutions coincide.

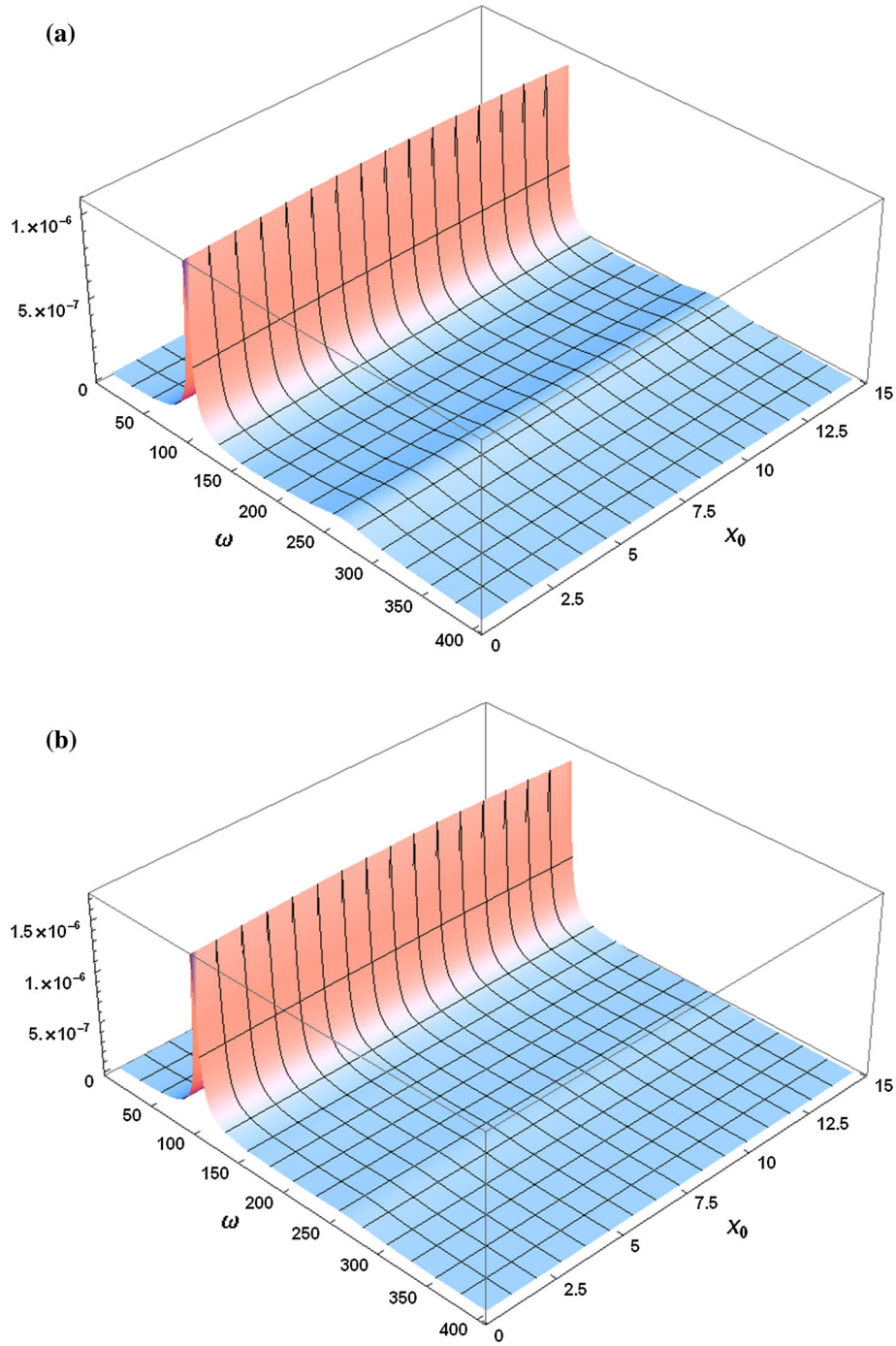

Fig. 8 Dynamic Green's function of the bar in Fig. 2 for a point load with varying forcing frequency ω and varying load position x_0: **a** axial displacement at midspan $x = L/2$; **b** axial displacement of mass damper at $x = L/3$

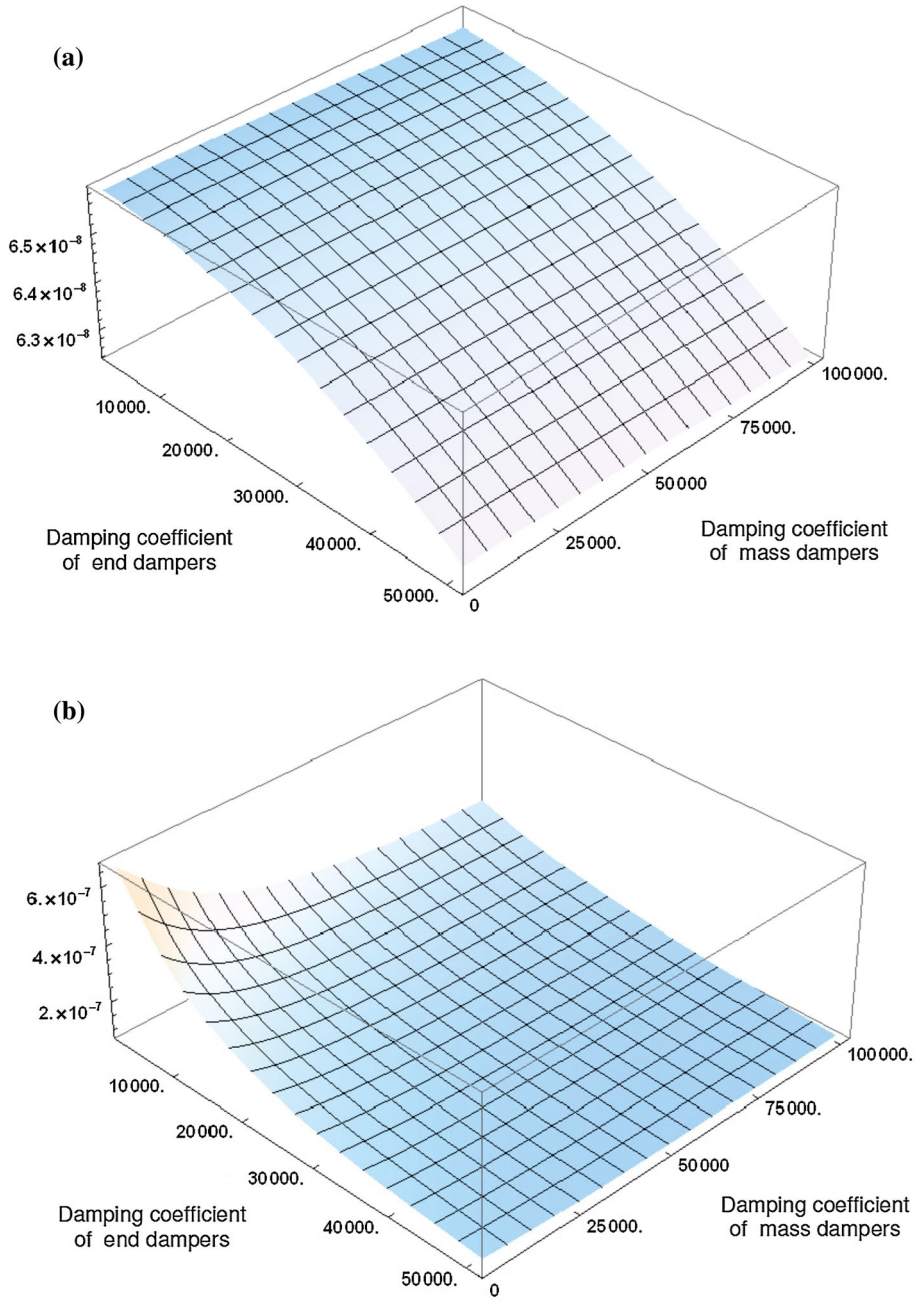

Fig. 9 Axial displacement frequency response function at midspan of the bar in Fig. 2 for a uniform load over $[L/6, 5L/6]$ for varying damping coefficients of end dampers and mass dampers: **a** forcing frequency $\omega = 50$ rad/s; **b** forcing frequency $\omega = 100$ rad/s

Table 4 Elements of dynamic stiffness matrix and load vector for the bar in Fig. 2

$\omega = 60$ rad/s		
	Eq. (30)	Eq. (B.6)
$(\mathbf{D}(\omega))_{1,1}$	$2.50840 \times 10^6 + 50111.30\,\mathrm{i}$	$2.50840 \times 10^6 + 50111.30\,\mathrm{i}$
$(\mathbf{D}(\omega))_{1,2} = (\mathbf{D}(\omega))_{2,1}$	$-6.88967 \times 10^6 - 2890.48\,\mathrm{i}$	$-6.88967 \times 10^6 - 2890.48\,\mathrm{i}$
$(\mathbf{D}(\omega))_{2,2}$	$2.50840 \times 10^6 + 50111.30\,\mathrm{i}$	$2.50840 \times 10^6 + 50111.30\,\mathrm{i}$
$\omega = 60$ rad/s—uniform load		
	Eq. (32)	Eq. (B.7)
$(\mathbf{f}_0(\omega))_{,1}$	$-0.72596 + 0.0037552\,\mathrm{i}$	$-0.72596 + 0.0037552\,\mathrm{i}$
$(\mathbf{f}_0(\omega))_{,2}$	$-0.72596 + 0.0037552\,\mathrm{i}$	$-0.72596 + 0.0037552\,\mathrm{i}$

6 Conclusions

This paper has addressed the frequency response of bars under harmonically varying point/polynomial loads, carrying multiple external/internal dampers at the same position, which may model external damping devices and internal damping due to damage or imperfect connections. Specifically, a method recently proposed by one of the authors for the bending response of Euler–Bernoulli beams [35] has been extended to axial response. In addition, an original formulation of exact dynamic stiffness matrix and load vector has been proposed, with advantages over a previous one [35].

The proposed solutions are obtained for all response variables, i.e. axial displacement and force. They are exact, fulfil the required conditions at the locations of dampers/point load, and can readily be implemented for any number and positions of dampers, positions of point/polynomial loads, with significant advantages over the exact classical approach and the standard FE method. For this, the proposed solutions appear particularly suitable for investigating the frequency response as dampers/load change position, as is typical in identification or optimization problems.

Acknowledgments The financial support of "PRIN 2010-2011: Dinamica, stabilità e controllo di strutture flessibili", Principal Investigator Prof. Luongo, is gratefully acknowledged.

Appendix 1

This Appendix provides analytical expressions for all terms in Eqs. (10–12).

Exact expressions in Eqs. (10–11)

The terms of matrix $\mathbf{\Omega}(x)$ in Eq. (10) and vectors $\mathbf{J}^{(P)}\left(x, x_j\right)$, $\mathbf{J}^{(\Delta U)}\left(x, x_j\right)$ in Eq. (11) can be derived as follows.
First, consider the steady-state motion equations of the bar under a harmonic unit point load and unit relative displacement at $x = x_0$, given as

$$\begin{aligned} \frac{\bar{\mathrm{d}}N(x)}{\mathrm{d}x} &= -m_0\omega^2 U(x) - P \cdot \delta(x - x_0), \quad P = 1, \\ \frac{\bar{\mathrm{d}}U(x)}{\mathrm{d}x} &= \frac{N(x)}{EA} + \Delta U \cdot \delta(x - x_0), \quad \Delta U = 1. \end{aligned} \tag{A.1.1,2}$$

From Eqs. (A.1.1,2), the following equation can be derived:

$$EA\frac{\bar{\mathrm{d}}^2 U(x)}{\mathrm{d}x^2} + m_0\omega^2 U(x) + P \cdot \delta(x - x_0) - EA \cdot \Delta U \cdot \delta^{(1)}(x - x_0) = 0 \tag{A.2}$$

with $P = 1$ and $\Delta U = 1$. On integrating by parts Eq. (A.2), it is noted that the following relation holds between the particular solutions $J_U^{(P)}(x, x_0)$ and $J_U^{(\Delta U)}(x, x_0)$, due to a unit point load $1 \cdot \delta(x - x_0)$ and unit relative displacement $1 \cdot \delta^{(1)}(x - x_0)$, respectively:

$$J_U^{(\Delta U)}(x, x_0) = -EA \int_0^L J_U^{(P)}(x, \xi)\, \delta^{(1)}(\xi - x_0)\, \mathrm{d}\xi = EA \frac{\bar{d} J_U^{(P)}(x, x_0)}{dx_0}. \tag{A.3}$$

The solution of the homogeneous equation associated with Eq. (A.2) and the particular integral $J_U^{(P)}(x, x_0)$ due to a unit point load are readily available in a closed form [26]. Starting from these solutions, and using Eqs. (A.1–A.3), terms in matrix $\mathbf{\Omega}(x)$ and vectors $\mathbf{J}^{(P)}\left(x, x_j\right)$ and $\mathbf{J}^{(\Delta U)}\left(x, x_j\right)$ are then obtained as

$$\begin{aligned} &\Omega_{U1}(x) = \cos(\eta(x - x_0)), && \Omega_{U2}(x) = \sin(\eta(x - x_0)), \\ &\Omega_{N1}(x) = -EA \cdot \eta \sin(\eta(x - x_0)), && \Omega_{N2}(x) = EA \cdot \eta \cos(\eta(x - x_0)) \end{aligned} \tag{A.4.1–4}$$

and

$$J_U^{(P)}(x, x_0) = -\rho \sin(\eta(x - x_0))\, H(x - x_0), \tag{A.5}$$

$$J_N^{(P)}(x, x_0) = EA \frac{\bar{\mathrm{d}} J_U^{(P)}(x, x_0)}{dx} = -\cos(\eta(x - x_0))\, H(x - x_0), \tag{A.6}$$

$$J_U^{(\Delta U)}(x, x_0) = \cos(\eta(x - x_0))\, H(x - x_0), \tag{A.7}$$

$$J_N^{(\Delta U)}(x, x_0) = EA \frac{\bar{\mathrm{d}} J_U^{(\Delta U)}(x, x_0)}{dx} - EA \cdot \delta(x - x_0) = -EA \cdot \eta \sin(\eta(x - x_0))\, H(x - x_0) \tag{A.8}$$

where $\eta = \eta(\omega) = EA^{-1/2} m_0^{1/2} \omega$ and $\rho = \rho(\omega) = EA^{-1/2} m_0^{-1/2} \omega^{-1}$. Recognize that the particular solutions are discontinuous where expected, i.e.

$$J_N^{(P)}\left(x_0^+, x_0\right) - J_N^{(P)}\left(x_0^-, x_0\right) = -1, \tag{A.9}$$

$$J_U^{(\Delta U)}\left(x_0^+, x_0\right) - J_U^{(\Delta U)}\left(x_0^-, x_0\right) = 1. \tag{A.10}$$

Exact expressions in Eq. (12)

Next, consider Eq. (12) for $\mathbf{Y}^{(f)}(x)$, which represents the particular solutions related to the applied load. In view of the analytical expressions of $\mathbf{J}^{(P)}(x, \xi)$ given in this Appendix, it can be seen that every integral in Eq. (12) can be reverted to the general form $\int_a^b g(\xi)\, H(x - \xi)\, d\xi$, with $g(\xi)$ given by the product of the loading function and certain trigonometric functions. For instance, in view of Eq. (A.5) for $J_U^{(P)}(x, x_0)$, computing $\mathbf{Y}^{(f)}(x)$ will involve, among others, the integral

$$\int_a^b J_U^{(P)}(x, \xi)\, f(\xi)\, \mathrm{d}\xi = \int_a^b g(\xi)\, H(x - \xi)\, \mathrm{d}\xi,\ g(\xi) = f(\xi)\, \rho \sin(\eta(x - x_0)). \tag{A.11}$$

Using the theory of generalized functions [45], $\int_a^b g(\xi)\, H(x - \xi)\, \mathrm{d}\xi$ can be computed as:

$$\begin{aligned} \int_a^b g(\xi)\, H(x - \xi)\, \mathrm{d}\xi &= \left\{H(x - \xi)\left[g^{[1]}(\xi) - g^{[1]}(x)\right]\right\}_a^b \\ &= H(x - b)\left[g^{[1]}(b) - g^{[1]}(x)\right] - H(x - a)\left[g^{[1]}(a) - g^{[1]}(x)\right] \end{aligned} \tag{A.12}$$

where $g^{[1]}$ denotes the first-order primitive function of $g(\xi)$. It is noticed that, for polynomial loads $f(x)$ typically encountered in engineering applications, the first-order primitive $g^{[1]}$ can be obtained in a closed form by any symbolic package [46]. This means that, upon deriving closed-form expressions of $\mathbf{c}$ from Eqs. (24), (21) provides the exact closed-form expressions of the FRFs for the bar with an arbitrary number of dampers, due to polynomial loads $f(x)\, e^{\mathrm{i}\omega t}$, for all the response variables.

Appendix 2

The exact dynamic stiffness matrix (30) and load vector (32) can be derived by the alternative procedure in Ref. [26,35], here recalled for convenience.

Equation (21) for the frequency response can be used to build the nodal equations

$$\mathbf{u} = \mathbf{\Gamma c} + \tilde{\mathbf{u}}^{(f)}, \tag{B.1}$$

$$\mathbf{f} = \mathbf{\Xi c} + \tilde{\mathbf{f}}^{(f)} \tag{B.2}$$

for $\mathbf{u}^{(f)} = \left[\, \tilde{U}^{(f)}(0)\ \tilde{U}^{(f)}(L), \right]^T$, $\mathbf{f}^{(f)} = \left[\, \tilde{N}^{(f)}(0)\ \tilde{N}^{(f)}(L) \,\right]^T$, $\mathbf{c} = \left[\, c_1\ c_2 \,\right]^T$, while $\mathbf{\Gamma}$ and $\mathbf{\Xi}$ are

$$\mathbf{\Gamma} = \begin{bmatrix} \left(\tilde{\mathbf{Y}}(0)\right)_{1,1} & \left(\tilde{\mathbf{Y}}(0)\right)_{1,2} \\ \left(\tilde{\mathbf{Y}}(L)\right)_{1,1} & \left(\tilde{\mathbf{Y}}(L)\right)_{1,2} \end{bmatrix}, \tag{B.3}$$

$$\mathbf{\Xi} = \begin{bmatrix} -\left(\tilde{\mathbf{Y}}(0)\right)_{2,1} & -\left(\tilde{\mathbf{Y}}(0)\right)_{2,2} \\ \left(\tilde{\mathbf{Y}}(L)\right)_{2,1} & \left(\tilde{\mathbf{Y}}(L)\right)_{2,2} \end{bmatrix} \tag{B.4}$$

where $\left(\tilde{\mathbf{Y}}(\cdot)\right)_{i,j}$ denotes the (i, j) element of matrix $\tilde{\mathbf{Y}}(x)$ in Eq. (21). From Eqs. (B.1–B.2) the following nodal matrix relation can be derived:

$$\mathbf{f} = \mathbf{\Xi\Gamma}^{-1}\left(\mathbf{u} - \tilde{\mathbf{u}}^{(f)}\right) + \tilde{\mathbf{f}}^{(f)} = \mathbf{D}(\omega)\,\mathbf{u} + \mathbf{f}_0 \tag{B.5}$$

where

$$\mathbf{D}(\omega) = \mathbf{\Xi\Gamma}^{-1}, \tag{B.6}$$

$$\mathbf{f}_0 = -\mathbf{\Xi\Gamma}^{-1}\tilde{\mathbf{u}}^{(f)} + \tilde{\mathbf{f}}^{(f)}. \tag{B.7}$$

In Eqs. (B.6–B.7), $\mathbf{D}(\omega)$ and $\mathbf{q}$ are the exact dynamic stiffness matrix and exact load vector of the bar in Fig. 1. Numerical applications of this paper show that Eq. (B.6) coincides with Eq. (30), while Eq. (B.7) coincides with Eq. (32). Upon deriving the nodal displacements, the frequency response in every member is computed from Eq. (21), where the vector of integration constants is back-calculated from the nodal displacements using the following expression:

$$\mathbf{c} = \mathbf{\Gamma}^{-1}\left(\mathbf{u} - \tilde{\mathbf{u}}^{(f)}\right). \tag{B.8}$$

References

1. Genta, G.: Vibration of Structures and Machines: Practical Aspects. Springer, New York (1995)
2. Housner, G.W., Bergman, L.A., Caughey, T.K., Chassiakos, A.G., Claus, R.O., Masri, S.F., et al.: Structural control: past, present, and future. J. Eng. Mech. **123**, 897–971 (1997)
3. Soong, T.T., Spencer Jr., B.F.: Supplemental energy dissipation: state-of-the-art and state-of-the-practice. Eng. Struct. **24**, 243–59 (2002)
4. Banerjee, J.R.: Dynamic stiffness formulation for structural elements: a general approach. Comput. Struct. **63**, 101–103 (1997)
5. Li, L., Hu, Y., Wang, X.: Eliminating the modal truncation problem encountered in frequency responses of viscoelastic systems. J. Sound Vib. **333**, 1182–1192 (2014)
6. Li, L., Hu, Y., Wang, X., Lü, L.: A hybrid expansion method for frequency response functions of non-proportionally damped systems. Mech. Syst. Signal Pr. **42**, 31–41 (2014)
7. Ou, J.P., Long, X., Li, Q.S.: Seismic response analysis of structures with velocity-dependent dampers. J. Constr. Steel Res. **63**, 628–638 (2007)
8. Tributsch, A., Adam, C.: Evaluation and analytical approximation of Tuned Mass Damper performance in an earthquake environment. Smart. Struct. Syst. **10**, 155–179 (2012)
9. Kareem, A., Kline, S.: Performance of multiple mass dampers under random loading. J. Struct. Eng. **121**, 348–361 (1995)

10. Lewandowski, R., Grzymislawska, J.: Dynamic analysis of structures with multiple tuned mass dampers. J. Civ. Eng. Manag. **15**, 77–86 (2009)
11. Oliveto, G., Santini, A., Tripodi, E.: Complex modal analysis of a flexural vibrating beam with viscous end conditions. J. Sound Vib. **200**, 327–345 (1997)
12. Xu, Y.L., Zhang, W.S.: Modal analysis and seismic response of steel frames with connection dampers. Eng. Struct. **23**, 385–396 (2001)
13. Kawashima, S., Fujimoto, T.: Vibration analysis of frames with semi-rigid connections. Comput. Struct. **19**, 85–92 (1984)
14. Sekulovic, M., Salatic, R., Nefovska, M.: Dynamic analysis of steel frames with flexible connections. Comput. Struct. **80**, 935–955 (2002)
15. Sarvestan, V., Mirdamadi, H.R., Ghayour, M., Mokhtari, A.: Spectral finite element for vibration analysis of cracked viscoelastic Euler–Bernoulli beam subjected to moving load. Acta Mech. **226**, 4259–4280 (2015)
16. Shafiei, M., Khaji, N.: Analytical solutions for free and forced vibrations of a multiple cracked Timoshenko beam subject to a concentrated moving load. Acta Mech. **221**, 79–97 (2011)
17. Caddemi, S., Morassi, A.: Multi-cracked Euler–Bernoulli beams: mathematical modeling and exact solutions. Int. J. Solids Struct. **50**, 944–956 (2013)
18. Caddemi, S., Caliò, I.: Exact reconstruction of multiple concentrated damages on beams. Acta Mech. **225**, 3137–3156 (2014)
19. Aso, K., Kan, K., Doki, H., Iwato, K.: Effects of vibration absorbers on the longitudinal vibration of a pipe string in the deep sea—part 1: in case of mining cobalt crust. Int. J. Offshore Polar Eng. **2**, 309–317 (1992)
20. Feng, Q., Shinozuka, M.: Control of seismic response of bridge structures using variable dampers. J. Intell. Mater. Syst. Struct. **4**, 117–122 (1993)
21. Argatov, I., Butcher, E.A.: On the separation of internal and boundary damage in slender bars using longitudinal vibration frequencies and equivalent linearization of damaged bolted joint response. J. Sound Vib. **330**, 3245–3256 (2011)
22. Hanss, M., Oexl, S., Gaul, L.: Identification of a bolted-joint model with fuzzy parameters loaded normal to the contact interface. Mech. Res. Commun. **29**, 177–187 (2002)
23. Butcher, E.A., Sevostianov, I., Burton, T.: On the separation of internal and boundary damage from combined measurements of electrical conductivity and vibration frequencies. Int. J. Eng. Sci. **46**, 968–975 (2008)
24. Ibrahim, R.A., Pettit, C.L.: Uncertainties and dynamic problems of bolted joints and other fasteners. J Sound Vib. **279**, 857–936 (2005)
25. Hull, A.J.: A closed form solution of a longitudinal bar with a viscous boundary condition. J. Sound Vib. **169**, 19–28 (1994)
26. Failla, G.: An exact generalised function approach to frequency response analysis of beams and plane frames with the inclusion of viscoelastic damping. J. Sound Vib. **360**, 171–202 (2016)
27. Alati, N., Failla, G., Santini, A.: Complex modal analysis of rods with viscous damping devices. J. Sound Vib. **333**, 2130–2163 (2014)
28. Hizal, N.A., Gürgöze, M.: Lumped parameter representation of a longitudinally vibrating elastic rod viscously damped in-span. J. Sound Vib. **216**, 328–336 (1998)
29. Yüksel, S., Gürgöze, M.: Continuous and discrete models for longitudinally vibrating elastic rods viscously damped in-span. J. Sound Vib. **257**, 996–1006 (2002)
30. Gürgöze, M., Erol, H.: On the eigencharacteristics of longitudinally vibrating rods carrying a tip mass and viscously damped spring-mass in-span. J. Sound Vib. **225**, 573–580 (1999)
31. Yüksel, S., Dalli, U.: Longitudinally vibrating elastic rods with locally and non-locally reacting viscous dampers. Shock Vib. **12**, 109–118 (2005)
32. Erol, H.: Characteristic equations of longitudinally vibrating rods carrying a tip mass and several viscously damped spring-mass systems in-span. Proc. Inst. Mech. Eng. Part C. J. Mech. Eng. Sci. **218**, 1–12 (2004)
33. Caddemi, S., Caliò, I., Cannizzaro, F.: Closed-form solutions for stepped Timoshenko beams with internal singularities and along-axis external supports. Arch. Appl. Mech. **83**, 559–577 (2013)
34. Xu, H., Li, W.L.: Dynamic behavior of multi-span bridges under moving loads with focusing on the effect of the coupling conditions between spans. J. Sound Vib. **312**, 736–753 (2008)
35. Failla, G.: Stationary response of beams and frames with fractional dampers via exact frequency response functions. J. Eng. Mech. doi:10.1061/(ASCE)EM.1943-7889.0001076
36. Yavari, A., Sarkani, S., Moyer, E.T.: On applications of generalized functions to beam bending problems. Int. J. Solids Struct. **37**, 5675–5705 (2000)
37. Yavari, A., Sarkani, S.: On applications of generalized functions to the analysis of Euler–Bernoulli beam-columns with jump discontinuities. Int. J. Mech. Sci. **43**, 1543–1562 (2001)
38. Falsone, G.: The use of generalised functions in the discontinuous beam bending differential equation. Int. J. Eng. Educ. **18**, 337–343 (2002)
39. Failla, G., Santini, A.: On Euler–Bernoulli discontinuous beam solutions via uniform-beam Green's functions. Int. J. Solids Struct. **44**, 7666–7687 (2007)
40. Failla, G., Santini, A.: A solution method for Euler–Bernoulli vibrating discontinuous beams. Mech. Res. Commun. **35**, 517–529 (2008)
41. Palmeri, A., Cicirello, A.: Physically-based Dirac's delta functions in the static analysis of multi-cracked Euler–Bernoulli and Timoshenko beams. Int. J. Solids Struct. **48**, 2184–2195 (2011)
42. Wang, J., Qiao, P.: Vibration of beams with arbitrary discontinuities and boundary conditions. J. Sound Vib. **308**, 12–27 (2007)
43. Guo, Y.Q., Chen, W.Q.: Dynamic analysis of space structures with multiple tuned mass dampers. Eng. Struct. **29**, 3390–3403 (2007)
44. Clough, R.W., Penzien, J.: Dynamics of Structures, 3rd edn. Computers and Structures Inc, Berkeley (1995)
45. Failla, G.: Closed-form solutions for Euler–Bernoulli arbitrary discontinuous beams. Arch. Appl. Mech. **81**, 605–628 (2011)
46. Mathematica. Version 7.0, Wolfram Research Inc., Champaign (2008)
47. Brandt, A.: Noise and Vibration Analysis: Signal Analysis and Experimental Procedures. Wiley, Chichester (2011)